THE JOURNAL OF PHYSICAL CHEMISTRY B

Article

pubs.acs.org/JPCB

# Physicochemical Properties of Three Ionic Liquids Containing a Tetracyanoborate Anion and Their Lithium Salt Mixtures

Nédher Sanchez-Ramirez,[†,⊥] Vitor L. Martins,[†,⊥] Rômulo A. Ando,[†] Fernanda F. Camilo,[‡] Sérgio M. Urahata,[§] Mauro C. C. Ribeiro,[†] and Roberto M. Torresi*[,†]

[†]Instituto de Química and [§]Instituto de Física, Universidade de São Paulo, C.P. 26077, CEP 05513-970, São Paulo, SP, Brazil

[‡]Instituto de Ciências Ambientais, Químicas e Farmacêuticas, Universidade Federal de São Paulo, Rua São Nicolau, 210, CEP 09913-030, Diadema, SP, Brazil

Supporting Information

**ABSTRACT:** Given their relevant physicochemical properties, ionic liquids (ILs) are attracting great attention as electrolytes for use in different electrochemical devices, such as capacitors, sensors, and lithium ion batteries. In addition to the advantages of using ILs containing lithium cations as electrolytes in lithium ion batteries, the $Li^+$ transport in ILs containing the most common anion, bis(trifluoromethanesulfonyl) imide anion ($[Tf_2N]$), is reportedly small; therefore, its contribution to the overall conductivity is also low. In this work, we describe the preparation and characterization of two new and one known IL containing the tetracyanoborate anion ($[B(CN)_4]$) as the anionic species. These ILs have high thermal and chemical stabilities, with almost twice the ionic conductivity of the $[Tf_2N]$ ILs and, most importantly, provide a greater role for the $Li^+$ ion throughout the conductivity process. The experimental ionic conductivity and self-diffusion coefficient data show that the $[B(CN)_4]$-based ILs and their $Li^+$ mixtures have a higher number of charge carriers. Molecular dynamics simulations showed a weaker interaction between $Li^+$ and $[B(CN)_4]$ than that with $[Tf_2N]$. These results may stimulate new applications for ILs that have good $Li^+$ transport properties.

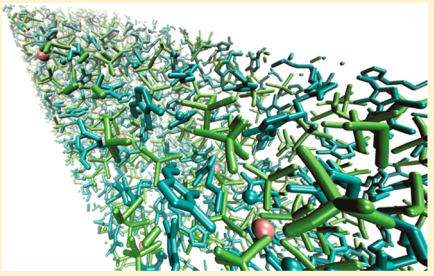

## INTRODUCTION

Ionic liquids (ILs) are salts with low melting points (typically below 373 K), and they have transport properties such as viscosity, conductivity, and an ionic diffusion coefficient that strongly depend on the nature of the ions (primarily on the charge distribution and size). They also exhibit high thermal stability, wide electrochemical stability, and low flammability and volatility; therefore, they can be considered a safer alternative to organic solvent-based electrolytes for use in various electrochemical devices such as capacitors, sensors, and lithium ion batteries.[1−9]

However, ILs that contain the anion most commonly used in electrochemical devices, the bis(trifluoromethanesulfonyl) imide anion ($[Tf_2N]$), exhibit strong coordinating properties due to the presence of oxygen atoms in their chemical structures.[10−12] Although these properties positively impact the solubility of lithium salts necessary for charge compensation in lithium ion batteries, they also have a detrimental effect on the transport properties of the IL, leading to fragility.[8,11,13] Thus, the increase in viscosity, decrease in conductivity, and formation of ionic aggregates must be minimized when a lithium salt is dissolved in the ILs to allow for their use as electrolytes in lithium ion batteries.[11]

The tetracyanoborate anion, $[B(CN)_4]$, has a negative charge uniformly delocalized over the four cyano groups that tetrahedrally surround the boron atom and has a weak ability to coordinate a cation,[14−18] primarily lithium, due to the absence of oxygen atoms in its structure. In addition, this anion has resistance to oxidation, and ILs containing $[B(CN)_4]$ exhibit a wide electrochemical window (EW), low viscosity, and high ionic conductivity that allow for their use as electrolytes in various electrochemical devices, particularly lithium ion batteries and supercapacitors.[19,20]

This paper reports the preparation and a detailed characterization of two new ILs, 1-*n*-butyl-2,3-dimethylimidazolium tetracyanoborate $[BMMI][B(CN)_4]$ and *N*-*n*-butyl-*N*-methylpiperidinium tetracyanoborate $[BMP][B(CN)_4]$, and a known IL that contains $[B(CN)_4]$, *N*-butyl-*N*-methylpyrrolidinium tetracyanoborate $[BMPyr][B(CN)_4]$, and their mixtures with lithium salts. The chemical structures of these three ILs are presented in Figure 1. This study was motivated by the reported stability of this new [BMMI]-containing IL toward Li that arises from the introduction of alkyl groups on the C-2 position of the imidazolium ring, which also increase its electrochemical stability.[21] The ILs with cyclic quaternary ammonium ions, such as pyrrolidinium and piperidinium cations, exhibit wider EWs, especially in the negative potential directions, than the imidazolium cation ILs. The wider EWs make these ILs suitable electrolytes for use in lithium ion batteries. We evaluated the fundamental characterization of these three ILs, including density, viscosity, thermal properties, ionic conductivity, and self-diffusion coefficients of the cations

**Received:** May 22, 2014
**Revised:** June 30, 2014
**Published:** July 3, 2014



   dx.doi.org/10.1021/jp505051v | J. Phys. Chem. B 2014, 118, 8772−8781

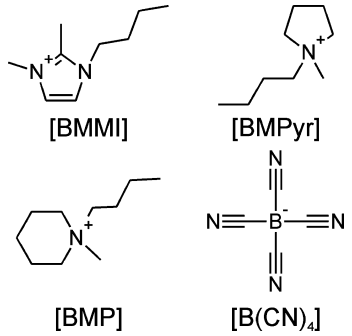


**Figure 1.** Schematic diagram of the constituent ions in the ILs studied: 1-*n*-butyl-2,3-dimethylimidazolium [BMMI], *N*-*n*-butyl-*N*-methylpiperidinium [BMP], *N*-*n*-butyl-*N*-methylpyrrolidinium [BMPyr], and tetracyanoborate [$B(CN)_4$].

and anions measured via pulsed gradient spin−echo nuclear magnetic resonance (PGSE-NMR), and we evaluated the local structure of one of these liquids and its $Li^+$ mixture by molecular dynamics (MD) simulations. Using these data, the pure ILs or their $Li^+$ salt mixtures can, for the first time, be compared with the respective systems containing the anion most commonly used in electrochemical devices, [$Tf_2N$]. It is worth noting that the amount of $Li^+$ salt that can be added to ILs containing the $[B(CN)]_4$ anion is much lower than that in ILs containing [$Tf_2N$] (0.1 versus more than 2.5 mol $L^{-1}$). This characteristic will be addressed in the discussion. These ILs exhibit less pronounced differences in the transport properties that result from the dissolution of a lithium salt ($Li[B(CN)_4]$) in comparison with the ILs containing [$Tf_2N$].

## EXPERIMENTAL METHODS

**Synthesis of $[B(CN)_4]$ Salts.** The procedure used to synthesize $KB(CN)_4$ has been described elsewhere.[22] $LiB(CN)_4$ was synthesized according to the procedure described in the literature.[23] Briefly, 5.00 g (32.0 mmol) of $KB(CN)_4$ dissolved in 20 mL of water reacted with 8.0 mL of 37% hydrochloric acid (96 mmol) and 8.0 mL of *n*-$Pr_3N$ (42 mmol). Then, the solid was extracted twice with 50 mL of $CH_2Cl_2$ each time, and the organic phase was dried using $MgSO_4$ and filtered. The filtrate was mixed with 20 mL of an aqueous solution containing 3.00 g of $LiOH{\cdot}H_2O$ (72 mmol), and the mixture was stirred vigorously for 1 h. All volatile products were removed under reduced pressure. $LiB(CN)_4$ was extracted from the residue with 50 mL of $CH_3CN$ in a Soxhlet apparatus, and the organic phase was evaporated out in a rotary evaporator. The crude product was recrystallized from water, washed with 50 mL of $CH_2Cl_2$, and freed from solvent residues under reduced pressure.

Compared with ILs containing a [$Tf_2N$] anion, the ILs containing anions with a cyanide group present higher toxicity. MSDS files from Merck Millipore and Sigma-Aldrich indicate that ILs containing the anions [$B(CN)_4$], [SCN], and [$N(CN)_2$] and the cation 1-butyl-1-methylimidazolium present high toxicity. It is important to point out that most cyanides compounds are toxic, mainly when dissolved in organic solvent; therefore, they should be handled with precaution.[23]

*$KB(CN)_4$ Data.* Elemental analysis data: Found: C: 31.1; N: 36.2. Calcd for $KB(CN)_4$: C: 31.1; N: 35.6; $\delta_C$ (75 MHz, $CD_3CN$, ppm): 121.9−124.7 (4C, q, $^1J_{BC}$ = 70.5 Hz) (Figure 1S, Supporting Information (SI)).

*$LiB(CN)_4$ Data.* Elemental analysis data: Found: C: 38.84; N: 44.63. Calcd for $LiB(CN)_4$: C: 39.44; N: 45.99.

**Syntheses of ILs Containing $[B(CN)_4]$.** In a flask, 3.50 g (230 mmol) of [BMP][Br] (IOLITEC, Germany) dissolved in 10 mL of water was added followed by 10 mL of an aqueous solution containing $KB(CN)_4$ (5.35 g, 230 mmol). The reaction mixture was stirred for 3 h at room temperature, and the two phases that formed were separated. The phase containing the IL was washed several times with water, treated with activated carbon, and run through a chromatography column (alumina, dichloromethane). The IL was dried under reduced pressure for 48 h at 80 °C to give [BMP][$B(CN)_4$] (3.94 g, 150 mmol, 64% yield) as a colorless liquid. [BMMI][$B(CN)_4$] and [BMPyr][$B(CN)_4$] were also synthesized from [BMMI][Br] and [BMPyr][Br] (IOLITEC, Germany), respectively, with similar a yield following the procedure above, and they were also obtained as colorless liquids, although [BMMI][$B(CN)_4$] presents a melting point of 63 °C. These ILs were stored under an argon atmosphere inside of a Labmaster glovebox ($H_2O$ < 1 ppm; $O_2$ < 10 ppm). The water content of these three ILs was measured using the standard coulometric Karl Fischer method (756 KF, Metrohm) and was estimated to be below 100 ppm for each.

The $Li^+$ mixtures with these ILs were prepared by adding the appropriate amount of $LiB(CN)_4$ in the ILs to obtain a concentration of 0.1 mol $L^{-1}$. The mixtures were maintained under agitation inside of the glovebox and went through the same drying process as the neat ILs. The final water concentration was estimated to be below 100 ppm. It is worth noting that it was not possible to obtain mixtures with a higher $Li^+$ concentration because further addition of $LiB(CN)_4$ causes it to precipitate.

The $Li^+$ mixtures with ILs containing the [$Tf_2N$] anion were prepared by adding the appropriate amount of Li[$Tf_2N$] (Aldrich) to the ILs [BMP][$Tf_2N$] and [BMPyr][$Tf_2N$] (IOLITEC, Germany) to obtain a concentration of 0.1 mol $L^{-1}$. The agitation and drying processes were carried out as explained above. The final water concentration was estimated to be below 100 ppm.

*[BMPyr][$B(CN)_4$] Data.* Elemental analysis data: Found: C: 59.7; H: 7.83; N: 26.9. Calcd for $C_{13}H_{22}N_5B$: C: 60.2; H: 7,84; N: 27.2; $\delta_H$ (300 MHz, $CD_3CN$, ppm): 0.97 (3H, t, $J$ = 7.5 Hz), 1.31−1.44 (2H, sextet, $J$ = 7.0 Hz), 1.67−1.77 (2H, m), 2.12−2.18 (4H, m), 2.93 (3H, s), 3.19−3.25(2H, m), and 3.33−3.45 (4H, m); $\delta_C$ (125 MHz, $CD_3CN$, ppm): 13.9, 20.4, 22.4, 26.3, 49.3, 65.1, 65.4, 122.4−124.1 (4C, q, $^1J_{BC}$ = 70.5 Hz) (Figures 2S and 3S, SI).

*[BMP][$B(CN)_4$] Data.* Elemental analysis data: Found: C: 61.5; H: 8.16; N: 25.8. Calcd for $C_{14}H_{22}N_5B$: C: 62.0; H: 8.18; N: 25.8; $\delta_H$ (300 MHz, $CD_3CN$, ppm): 0.95−1.00 (3H, t, $J$ = 7.5 Hz), 1.31−1.43 (2H, sextet, $J$ = 7.2 Hz), 1.57−1.73 (4H, m), 1.79−1.88 (4H, m), 2.92 (3H, s), and 3.18−3.25(6H, m); $\delta_C$ (75 MHz, $CD_3CN$, ppm): 13.8, 20.4, 20.5, 21.6, 24.3, 48.8, 62.1, 64.2, 121.9−124.7(4C, q, $^1J_{BC}$ = 70.5 Hz) (Figures 4S and 5S, SI).

*[BMMI][$B(CN)_4$] Data.* Elemental analysis data: Found: C: 58.1; H: 6.40; N: 30.6. Calcd for $C_{13}H_{17}N_6B$: C: 58.3; H: 6.31; N: 31.3; $\delta_H$ (300 MHz, $CD_3CN$, ppm): 0.93−0.97 (3H, t, $J$ = 6.0 Hz), 1.29−1.41 (2H, sextet, $J$ = 7.2 Hz), 1.69−1.79 (2H, q, $J$ = 7.5), 3.05 (3H, s), 3.69 (3H, s), 4.00−4.05(2H, t, $J$ = 7.5 Hz), and 7.23−7.26 (2H, m); $\delta_C$ (75 MHz, $CD_3CN$, ppm): 10.0, 13.7, 20.0, 32.2, 35.7, 49.0, 121.7, 123.1, 145.25, 121.7−124.5(4C, q,$^1J_{BC}$ = 70.5 Hz) (Figures 6S and 7S, SI).


dx.doi.org/10.1021/jp505051v | J. Phys. Chem. B 2014, 118, 8772−8781

**Measurements.** Density and viscosity measurements were performed with a thermoregulated digital densimeter/viscometer (SVM 3000/G2, Anton Paar K. G.)

Ionic conductivity was measured by the impedance method with an Autolab PGSTAT 30 (Eco Chemie) in the frequency range of 0.1−100 kHz. The cell constant was determined by using a standard KCl aqueous solution.

The electrochemical stabilities of the pure ILs were estimated by cyclic voltammetry using an Autolab PGSTAT 30 (Eco Chemie) with glassy carbon as the working electrode, Pt as the counter electrode, and Ag wire as a pseudoreference at 50 mV $s^{-1}$ and $j_{cut}$ = 150 mA $cm^{-2}$.

Differential scanning calorimetry (DSC) was carried out under a nitrogen atmosphere using a T. A. Instruments Q.10 DSC coupled with a T. A. refrigerated cooling system interfaced to the Thermal Analyst 2000 software. The samples for DSC measurements were sealed in an aluminum pan. First, the samples were cooled (10 °C $min^{-1}$) to −80 °C and then heated at a rate of 10 °C $min^{-1}$ back up to 300 °C.

Thermogravimetric (TG) measurements were performed under a nitrogen atmosphere in a Pt crucible using a T. A. Instruments Hi-ResTM TGA 2950 interfaced to the Thermal Analyst 2000 software. The measurements were conducted from room temperature to 800 °C at a heating rate of 10 °C $min^{-1}$ and with a resolution of 3 °C and sensitivity of 1 °C.

The Raman spectra of the samples were obtained in a FT-Raman Bruker RFS 100/S using the 1064 nm line of a Nd/YAG laser, which has a typical output power of 50 mW and a spectral resolution of 1.0 $cm^{-1}$.

Diffusion coefficients, $D$, were measured by pulsed gradient spin−echo nuclear magnetic resonance (PGSE-NMR) in a Varian INOVA 300 spectrometer equipped with a 5 mm indirect detection probe (22 G $cm^{-1}$ max) and calibrated with water ($D$ = 2.299 × $10^{-9}$ $m^2$ $s^{-1}$) at 298 K. A stimulated spin−echo pulse sequence, that is, 90° − $\tau_1$ − 90° − $\tau_2$ − 90° − $\tau_1$ − acquisition, incorporating a gradient pulse in each $\tau_1$ period, was used. Diffusion coefficients were obtained according to procedures described elsewhere.[10,11,24]

## COMPUTATIONAL DETAILS

The MD simulations were performed with a potential energy function that takes into account the intermolecular Lennard-Jones and Coulombic interactions, as well as the intramolecular properties of bond stretching $r$, angle bending $\theta$, and torsion of the dihedral angles $\psi$

$$V_{total} = \sum_{i,j;i<j} \left\{ 4\epsilon_{ij} \left[ \left(\frac{\sigma}{r_{ij}}\right)^{12} - \left(\frac{\sigma}{r_{ij}}\right)^{6} \right] + \frac{q_i q_j}{r_{ij}} \right\} + \sum_{bonds} k_b (r - r_{eq})^2 + \sum_{angles} k_\theta (\theta - \theta_{eq})^2 + \sum_{dihedrals} k_\psi [1 + \cos(n\psi - \delta)] \quad (1)$$

where $r_{ij}$ is the distance between atoms $i$ and $j$ of different ions. Parameters such as the bond lengths $r_{eq}$, the angles $\theta_{eq}$, the dihedral angles $\psi_{eq}$, and the force constant parameters are based on the models of Morrow et al.[25] and Monteiro et al.[10] for the [BMMI] cation (hydrogen is not explicit). The $[B(CN)_4]$ anion parameters were based on the FF-1 model from Koller et al.,[26] and the $[Tf_2N]$ anion and $Li^+$ parameters were taken from Monteiro et al.[10]

The simulations were conducted in cubic (neat IL) and rectangular ($Li^+$ mixture) boxes generated by Packmol[27] with a random configuration at 400 K to achieve significant ionic mobility and a proper statistical average. The number of molecules in each system is presented in Table 1S, SI.

Pre-equilibrium simulations were conducted, allowing the variation of the box size using a Berendsen's barostat to reach an average pressure of 0.1 MPa and the expected density for this temperature. The equilibration runs were longer than 2.0 ns with a time step of 5.0 fs. The production runs were longer than 5.0 ns with a time step of 5.0 fs in a *NVE* ensemble with an equation of motion integrated with the velocity Verlet algorithm[28] as the equilibration ran.

The common criterion of the total energy fluctuation was used to handle the energy conservation, $\Delta E(t) = [E(0) - E(t)]/E(0)$, where $E(t)$ is the total energy at time $t$ and $E(0)$ is the initial energy.[29] Further computational details are described in refs 10 and 30. The simulated systems exhibited satisfactory total energy conservation. Figure 8S in the SI represents the total energy fluctuations for the $[Li][BMMI][B(CN)_4]$ simulation. The similarity between the calculated and experimental density shows that the MD simulations yield reliable results regarding the local structure in the liquids.

The partial radial distribution functions (rdfs) were calculated by homemade routines, while the combined distribution functions (cdfs) and spatial distribution functions (sdfs) were calculated by the software package Travis.[31]

## RESULTS AND DISCUSSION

**Thermal and Electrochemical Stability.** Table 1 presents the thermal properties and electrochemical stability of the ILs studied in this work. TG analyses (see Figure 9S, SI) reveal that the first and unique thermal event upon heating these ILs is their thermal decomposition. Their decomposition temperatures ($T_d$) were above 400 °C, indicating a remarkable thermal stability. Similar thermal stabilities were expected because this property is fundamentally related to the anionic species. Compared with ILs containing $[Tf_2N]$,[21,32] the $[B(CN)_4]$-based ILs have a slightly higher $T_d$ because the $[B(CN)_4]$ anion is more stable than $[Tf_2N]$ at high temperature.[33] The melting points ($T_m$) were determined via DSC, and the endothermic melting events occurred at 21, 17, and 60 °C for $[BMPyr][B(CN)_4]$, $[BMP][B(CN)_4]$, and $[BMMI][B(CN)_4]$, respectively. The TG and DSC curves are shown in Figures 9S and 10S in the SI.

**Table 1. Thermal Properties and EW of the ILs**

| ILs | $T_m$/°C | $T_d$/°C | EW/V |
|---|---|---|---|
| $[BMPyr][B(CN)_4]$ | 21 | 403 | 4.8 |
| $[BMP][B(CN)_4]$ | 17 | 414 | 5.7 |
| $[BMMI][B(CN)_4]$[a] | 63 | 455 | 2.8 |

[a]The EW was obtained at 63 °C.

Given that the inductive effect uniformly delocalizes the negative charge on the $[B(CN)_4]$ anion over the four cyano groups, its electrochemical stability is expected to be superior to that of the $[Tf_2N]$ anion. Consequently, the observed EW (see Figure 11S, SI) values for the ILs containing [BMP], [BMPyr] cations, and $[B(CN)_4]$ were larger than those obtained for their $[Tf_2N]$ analogues. The relatively low EW observed in $[BMMI][B(CN)_4]$ is attributed to the experimental temperature. This higher electrochemical stability for quaternary


dx.doi.org/10.1021/jp505051v | J. Phys. Chem. B 2014, 118, 8772−8781

ammonium-based ILs relative to imidazolium-containing ILs has been previously described.[34]

**Density.** Figure 2 shows the densities of the neat ILs and their mixtures with $Li^+$ salt in a range of temperatures. The

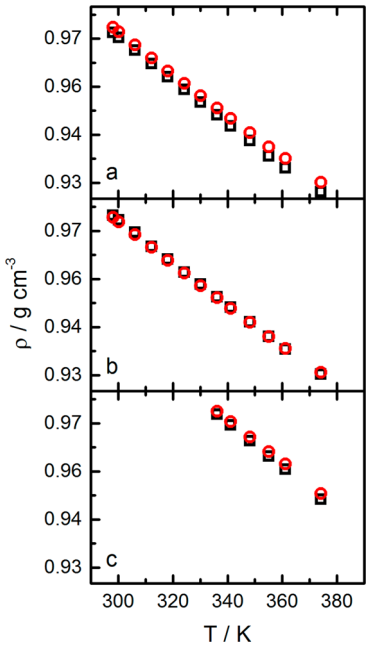


**Figure 2.** Density at different temperatures for neat ILs (open black squares) and their $Li^+$ mixtures (open red circles) for (a) [BMPyr][$B(CN)_4$], (b) [BMP][$B(CN)_4$], and (c) [BMMI][$B(CN)_4$].

densities exhibit practically a linear dependence with temperature and are lower than 1.0 g $cm^{-3}$ at room temperature (25 °C), which is much lower than in the [$Tf_2N$] analogues.[21,35] The anion [$B(CN)_4$] has a weaker coordinating ability than [$Tf_2N$]; therefore, the ionic system is less densely packed, increasing the molar volume.[36] The addition of $Li^+$ salt does not cause any considerable change in the density. It is also worth mentioning that the $Li^+$ concentration in the mixtures is 0.1 mol $L^{-1}$ because the addition of more $LiB(CN)_4$ causes it to precipitate.

Ye and Shreeve[37] proposed the following formula to calculate the theoretical density of several ILs

$$\rho_{calc} = \frac{W}{0.6022V} \quad (2)$$

where $W$ is the molar mass and $V$ the proposed ion volume. Given the volumes for [BMMI], [BMP], [BMPyr], [$B(CN)_4$], and [$Tf_2N$] of 266, 271, 253, 143, and 248 $Å^3$, respectively, the corresponding predicted density values for [BMPyr][$B(CN)_4$], [BMP][$B(CN)_4$], and [BMMI][$B(CN)_4$] are 1.078, 1.087, and 1.088 g $cm^{-3}$. The predicted $\rho_{calc}$ values for the ILs based on the [$B(CN)_4$] anion are slightly higher than the experimental values, compared to those for ILs containing [$Tf_2N$].[10,37] This deviation suggests that there is more free volume in the ILs containing [$B(CN)_4$] than in those based on [$Tf_2N$]. Therefore, their predicted densities taking into account the volume of the separated building blocks will be more distinctly higher than the experimental densities. This will be addressed in more detail in the MD Simulations results subsection.

**Viscosity and Ionic Conductivity.** Figure 3 shows the Arrhenius plot of viscosity for the neat ILs containing

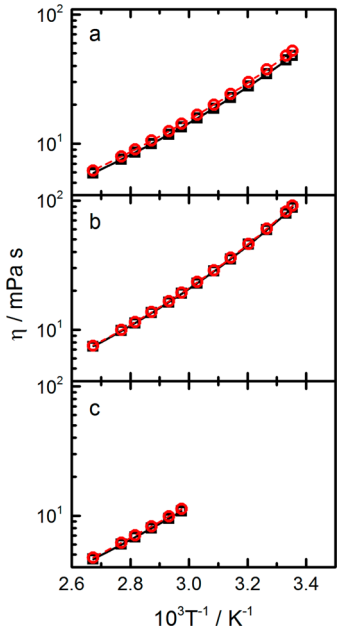


**Figure 3.** Arrhenius plots of the viscosity of neat ILs (open black squares) and their $Li^+$ mixtures (open red circles) for (a) [BMPyr][$B(CN)_4$], (b) [BMP][$B(CN)_4$], and (c) [BMMI][$B(CN)_4$]. Full black lines (neat ILs) and dashed red lines ($Li^+$ mixtures) represent the best fits of the VTF equation.

[$B(CN)_4$] and their respective $Li^+$ mixtures. It can be noted that the viscosity of the ILs and their $Li^+$ mixtures decreases with increasing temperature. The addition of $Li^+$ does not cause any considerable change in this property. The identities of the anion and the cation that compose the ILs are known to have a great effect on the viscosity of the IL. Thus, all ILs containing [$B(CN)_4$] are less viscous than their [$Tf_2N$] analogues.[21,32,38] The viscosities of the latter are approximately two times higher than those obtained for the [$B(CN)_4$] salts. This effect can be understood given that [$B(CN)_4$] has a negative charge delocalized by the strong electron-withdrawing effect of the four nitrile groups, as previously described in the explanation for the differences in densities.[16]

The lines in Figure 3 represent the best fits by the Vogel–Tammann–Fulcher (VTF) equation[39] for the viscosity, where $\eta_0$, $B$, and $T_0$ are the adjustable parameters whose values are shown in Table 2S (SI). Although the parameters for [BMMI][$B(CN)_4$] are shown, because of the short temperature range studied, the analyses will be restricted to the other two ILs. [BMMI][$B(CN)_4$] parameters were not determined due to the short temperature range studied. $T_0$ is the temperature at which the viscosity tends to infinity. The addition of $Li^+$ slightly increases $T_0$, indicating that the viscosity will reach infinity at a higher temperature than that for the neat IL. The relationship $B/T_0$ can be related to the fragility of the liquid or, in other words, how the transport properties vary with temperature change. The transport properties of strong liquids (low $B/T_0$) suffer less change with the temperature than do weak liquids (high $B/T_0$). For [BMPyr][$B(CN)_4$] and [BMP][$B(CN)_4$], $B/T_0$ is 4.8 and 4.2, respectively. These values are close to those of ILs based on the [$Tf_2N$] anion and the same cations,[21] indicating that both IL classes ([$Tf_2N$] and [$B(CN)_4$]) have similar fragility. The addition of $Li^+$ does not greatly alter the fragility of ILs containing the [$B(CN)_4$] anion (4.6 and 3.9 for mixtures with [BMPyr][$B(CN)_4$] and


dx.doi.org/10.1021/jp505051v | J. Phys. Chem. B 2014, 118, 8772–8781

[BMP][B(CN)$_4$], respectively). In contrast, in ILs based on the [Tf$_2$N] anion, the addition of Li$^+$ has a huge impact on the liquid fragility, leading to a weaker liquid in comparison with the neat IL.[10] This difference must be associated with a low Li$^+$ concentration. It is worth noting, however, that fragility analyses are usually made near the glass transition temperature, and in this work, we are considering the strong/fragile classification only in the temperature range studied here. A different $\eta(T)$ profile must be considered at a different range of temperatures.[40]

Figure 4 shows the Arrhenius plot of the ionic conductivity for the three neat ILs containing [B(CN)$_4$] and their Li$^+$

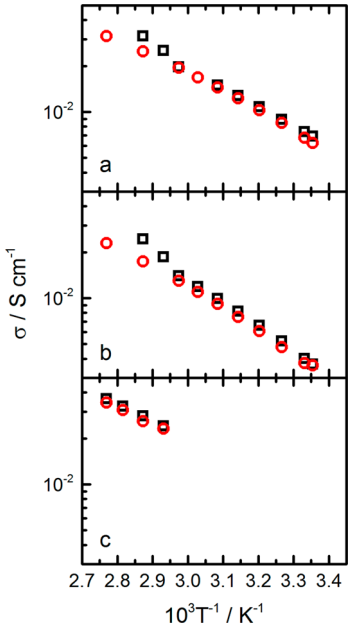


**Figure 4.** Arrhenius plots of the ionic conductivity of neat ILs (open black squares) and their Li$^+$ mixtures (open red circles) for (a) [BMPyr][B(CN)$_4$], (b) [BMP][B(CN)$_4$], and (c) [BMMI][B(CN)$_4$].

mixtures. The ionic conductivity values were found to be approximately three times greater than those for the [Tf$_2$N] analogues,[21,32,38] except for the [BMPyr] derivatives. This fact indicates that the decrease of the ionic conductivity in ILs containing [Tf$_2$N] cannot be completely attributed to the detrimental effect of the viscosity because the viscosity values of ILs based on [B(CN)$_4$] are approximately two times lower than those analogues containing [Tf$_2$N]. In other words, the increase in the ionic conductivity of the ILs containing [B(CN)$_4$] cannot be attributed solely to the resistance effect of the ions that is associated with the viscosity. Therefore, to explain this result, one must consider the actual concentration of the charge carriers in both types of ILs.

If one considers the density of each IL at each temperature and its molar mass, it is possible to calculate the ionic molarity, that is, the ion concentration, disregarding the aggregates with no charge. At room temperature, for example, [BMPyr][B(CN)$_4$] and [BMP][B(CN)$_4$] have ionic concentrations of 3.8 and 3.6 mmol cm$^{-3}$, respectively, and [BMMI][B(CN)$_4$] has an ionic concentration of 3.7 mmol cm$^{-3}$ at 64 °C. Considering this, it is possible to calculate the molar ionic conductivity.

Figure 5 presents the Walden plot, the logarithm of molar ionic conductivity as a function of the logarithm of fluidity (inverse of viscosity). The straight line from corner to corner

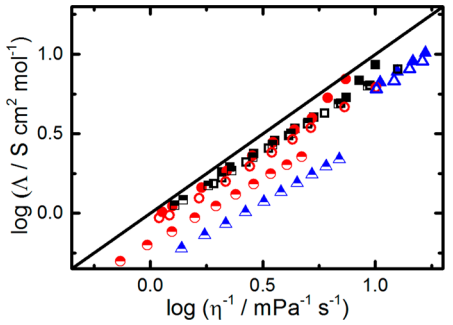


**Figure 5.** Walden plot of neat ILs and their Li$^+$-containing mixtures. [BMPyr][B(CN)$_4$] (■), [BMP][B(CN)$_4$] (red ●), [BMMI][B(CN)$_4$] (blue ▲), [Li][BMPyr][B(CN)$_4$] (□), [Li][BMPyr][B(CN)$_4$] (red ○), [Li][BMMI][B(CN)$_4$] (blue △), [BMPyr][Tf$_2$N] (⬒), [BMP][Tf$_2$N] (red ◓), and [BMMI][Tf$_2$N] (blue half shaded triangle).

(with a slope of one) is the ideal line for a classical dilute aqueous solution. Deviations from this line are related to the IL ionicity.[41−43] All of the systems analyzed here lie below the ideal line, indicating that these systems are not free of aggregates between cations and anions. The ILs [BMP][Tf$_2$N] and [BMMI][Tf$_2$N] are the most distant from the ideal line and exhibit lower ionicity. The ILs containing the [B(CN)$_4$] anion are closer to the ideal line because the weaker interaction between the cations and [B(CN)$_4$] guarantee a higher ionicity compared to the corresponding ILs with [Tf$_2$N]. The Li$^+$ mixture with the ILs containing the [B(CN)$_4$] anion shows a slight diminution of the ionicity.

Another way to present the Walden plot is shown in Figure 12S (SI), where the molar ionic conductivity is presented as a function of fluidity. In this case, the slope is related to the ionicity, with a larger slope signifying a larger ionicity. This is a good way to analyze how molar ionic conductivity varies with viscosity and takes into account the formed aggregates. [BMPyr][B(CN)$_4$] and [BMP][B(CN)$_4$] show a similar slope (65 and 72 S cm$^{-2}$ mol$^{-1}$ mPa$^{-1}$ s$^{-1}$, respectively), indicating that the increase in molar ionic conductivity in both ILs is related equally to the decrease in viscosity or increase in fluidity. On the other hand, [BMMI][B(CN)$_4$] has a slope of 57 S cm$^{-2}$ mol$^{-1}$ mPa$^{-1}$ s$^{-1}$, slight lower than that of the other two ILs. This indicates that the IL containing [BMMI] should form more aggregates with no formal charge or bigger aggregates than the ILs containing [BMPyr] and [BMP]. Comparing the slope of the Walden plot for the ILs containing [B(CN)$_4$] with that of the analogues containing [Tf$_2$N], it is possible to observe the huge difference in the behavior of aggregate formation when each anion is present. Besides the similarity between the analogues containing the [BMPyr] cation (slope of 65 S cm$^{-2}$ mol$^{-1}$ mPa$^{-1}$ s$^{-1}$ for the [Tf$_2$N]-containing IL),[32,38,44] the ILs [BMP][Tf$_2$N] and [BMMI][Tf$_2$N] have very different slopes, 47[21] and 31[21] S cm$^{-2}$ mol$^{-1}$ mPa$^{-1}$ s$^{-1}$, respectively. We can infer that the ILs based on [B(CN)$_4$] have weaker interactions with the cations and that the charge carriers are more free in these systems, resulting in higher molar ionic conductivity as a function of fluidity. As Figure 5 already indicated, Figure 12S (SI) also suggested a similarity between the ionicity of the ILs [BMPyr][B(CN)$_4$] and [BMPyr][Tf$_2$N].

**Diffusion Coefficients.** Another way to analyze how the ions are contributing to the ionic conductivity is to evaluate the self-diffusion coefficients. Figure 6 shows the self-diffusion


dx.doi.org/10.1021/jp505051v | J. Phys. Chem. B 2014, 118, 8772−8781

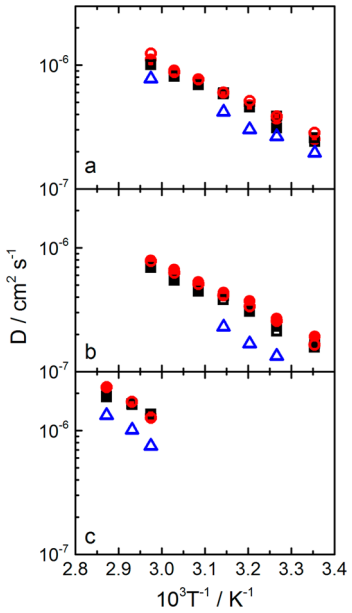


**Figure 6.** Arrhenius plots of self-diffusion coefficients. (a) [BMPyr]-[$B(CN)_4$]: [BMPyr] (full black square) and [$B(CN)_4$] (full red circle). [Li][BMPyr][$B(CN)_4$]: [BMPyr] (open black square), [$B(CN)_4$] (open red circle), and $Li^+$ (open blue triangle). (b) [BMP][$B(CN)_4$]: [BMP] (full black square) and [$B(CN)_4$] (full red circle). [Li][BMP][$B(CN)_4$]: [BMP] (open black square), [$B(CN)_4$] (open red circle), and $Li^+$ (open blue triangle). (c) [BMMI][$B(CN)_4$]: [BMMI] (full black square) and [$B(CN)_4$] (full red circle). [Li][BMMI][$B(CN)_4$]: [BMMI] (open black square), [$B(CN)_4$] (open red circle), and $Li^+$ (open blue triangle).

coefficients for each ion in the neat ILs and their corresponding $Li^+$ mixtures, which were determined via PGSE-NMR. This technique allows the diffusivity of each ionic species to be determined independently,[45−47] with the $^{11}B$, $^1H$, and $^7Li$ nuclei used to detect the [$B(CN)_4$] anion, organic cations, and $Li^+$, respectively. For all ILs containing [$B(CN)_4$], the cation and anion diffusion coefficients increased almost 2-fold over those obtained for the [$Tf_2N$]-based ILs,[10,21] in accordance with the change in viscosity. The $Li^+$ diffusion coefficients are smaller when compared with the $D_c$ and $D_a$ values obtained for the same mixture, indicating that among all species, $Li^+$ diffuses more slowly. In addition, for the ILs containing [$B(CN)_4$] mixtures, $D_{Li+}$ is approximately 20% smaller than $D_c$ and $D_a$, whereas this difference is approximately 50% for the ILs containing [$Tf_2N$].[10]

The Stokes−Einstein equation presents the relationship between the diffusion and viscosity, $D \propto \eta^{-1}$, and we can use this relationship to compare the relaxation between both transport properties. Figure 13S (SI) shows the plot of the self-diffusion coefficients as a function of the fluidity ($\eta^{-1}$) for the neat ILs and their $Li^+$ mixtures. As this relationship is linear for all systems, it is possible to affirm that both transport properties present similar relaxation processes. Thus, the increase of the self-diffusion coefficients with the increment in temperature is straight related with the increase of the fluidity, that is, the decrease of viscosity.

From the self-diffusion coefficients, it is possible to estimate the $\Lambda_{NMR}$ values using the Nernst−Einstein equation (see Figure 14S, SI). The $\Lambda_{NMR}$ values were higher than the experimental ones, $\Lambda_{exp}$, for all ILs. The ratio between these values ($\Lambda_{exp}/\Lambda_{NMR}$) was examined to obtain further insight into the equilibrium ionic dissociation/association in the ILs (Figure 7). The actual percentage of ions that contribute to the molar

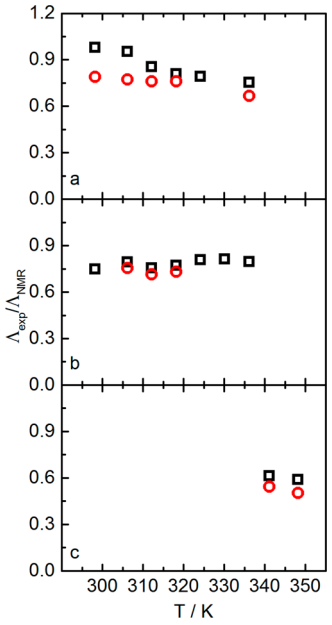


**Figure 7.** Ratio of the measured and calculated (by NMR) molar ionic conductivity ($\Lambda_{exp}/\Lambda_{NMR}$) of the neat ILs (open black squares) and their $Li^+$ mixtures (open red circles) for (a) [BMPyr][$B(CN)_4$], (b) [BMP][$B(CN)_4$], and (c) [BMMI][$B(CN)_4$].

ionic conductivity for each family of anionic ILs was estimated. If all charge carriers were available for conduction, the $\Lambda_{exp}/\Lambda_{NMR}$ ratio would equal to 1; however, if $\Lambda_{exp}/\Lambda_{NMR} < 1$, a portion of the mobile species detected in the PGSE experiments would not contribute to the conductivity. By comparing a pair that contains the same cationic species (e.g., [BMMI][$B(CN)_4$] versus [BMMI][$Tf_2N$][21]), one can confirm that the [$B(CN)_4$] anion contributes to the increase of $\Lambda_{exp}/\Lambda_{NMR}$, which suggests that a higher percentage of ions contributes to the ionic conductivity. This difference can be explained from a structural and electronic standpoint; the extensively delocalized negative charge on the [$B(CN)_4$] coupled with the weak coordination of the anion diminishes the interactions between the ions, leaving them less tightly bound and increasing the value of $\Lambda_{exp}/\Lambda_{NMR}$.

Adding a lithium salt to an IL containing [$Tf_2N$] is known to have a detrimental effect on its transport properties, leading to a substantial decrease in conductivity and an increase in viscosity and density.[10,11] This effect demonstrates that these ILs are fragile and that the strong Lewis acid character of the $Li^+$ modifies the ILs, creating a tight short-range structure. In this IL family, the $Li^+$ cations are coordinated by the oxygen atoms from the surrounding anion to form clusters. Thus, the contribution of the $Li^+$ to the ionic conductivity does not increase proportionally to the $Li^+$ concentration. The $\Lambda_{exp}/\Lambda_{NMR}$ values for the mixture containing 0.1 mol $L^{-1}$ $LiB(CN)_4$ are similar to those obtained for the pure ILs, which is attributed to the small $Li^+$ salt concentration when compared with other results in which the $Li^+$ salt concentrations were 1 or 2 mol $L^{-1}$.[10,11] However, if one compares these $Li^+$ mixtures containing [$B(CN)_4$] with similar mixtures containing the [$Tf_2N$] (0.1 mol $L^{-1}$ $LiTf_2N$) at 25 °C, it is possible to observe that the $Li^+$ ion has a more important contribution to the ionic


dx.doi.org/10.1021/jp505051v | J. Phys. Chem. B 2014, 118, 8772−8781

conductivity for mixtures containing $[B(CN)_4]$ than the mixtures containing $[Tf_2N]$, 0.066 versus 0.034 mS $cm^{-1}$ for $[BMPyr][B(CN)_4]$ and $[BMPyr][Tf_2N]$ and 0.044 versus 0.017 mS $cm^{-1}$, for $[BMP][B(CN)_4]$ and $[BMP][Tf_2N]$. All of the data analyzed for these mixtures are shown in Tables 3S and 4S in the SI.

**Raman Spectroscopy.** Raman spectroscopy has been used to examine structural changes as a function of the $Li^+$ concentration in several IL systems.[10,48,49] In IL mixtures containing $[Tf_2N]$, the most sensible Raman band used to evaluate the formation of ionic pairs in these systems is the vibrational mode of $[Tf_2N]$ located at 740 $cm^{-1}$.[48,50] This single band located at 740 $cm^{-1}$ for neat ILs reportedly turns into a doublet at 740 and 747 $cm^{-1}$ when a $Li^+$ salt is added. This shift and split is attributed to the formation of ion pairs or aggregates due to the coordination of $Li^+$ by the $[Tf_2N]$ anion. Therefore, evaluating these two bands allows the study of the formation of aggregates between $Li^+$ and $[Tf_2N]$ anions (at 747 $cm^{-1}$) and those related to the interactions between the organic cation and $[Tf_2N]$ (at 740 $cm^{-1}$).[10,48,49] In the ILs containing $[B(CN)_4]$, Raman spectroscopy is also useful, but the region of focus becomes 2200−2300 $cm^{-1}$, at which the C≡N stretching occurs.[51]

Figure 8 provides the Raman spectra in the region of the C≡N vibrational modes of $Li[B(CN)_4]$ (black line, open circles),

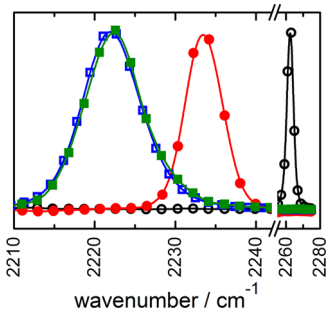


**Figure 8.** Raman spectra of $LiB(CN)_4$ (black line, open circles), $KB(CN)_4$ (red line, solid circles), $[BMPyr][B(CN)_4]$ (blue line, open squares), and $[Li][BMPyr][B(CN)_4]$ (green line, solid squares).

$KB(CN)_4$ (red line, solid circles), $[BMP][B(CN)_4]$ (blue line, open squares), and $[BMPyr][B(CN)_4]$ + 0.1 mol $L^{-1}$ $LiB(CN)_4$ (green line, solid squares). When the Lewis acid strength of the cation diminishes, the band corresponding to the $\nu$(C≡N) stretching mode clearly shifts to lower wavenumbers, 2262.4 $cm^{-1}$ for $Li[B(CN)_4]$, 2233.4 $cm^{-1}$ for $K[B(CN)_4]$, and 2222.2 $cm^{-1}$ for $[BMPyr][B(CN)_4]$. Such behavior has previously been observed for a series of $[B(CN)_4]$ salts, including ILs, and follows a well-established trend according to the charge/radius ratio.[23,51] When $Li[B(CN)_4]$ is added to the neat IL, the band assigned to $\nu$(C≡N) shifts to slightly higher wavenumbers, indicating a weak interaction between the $Li^+$ and $[B(CN)_4]$. This behavior is different from that observed for ILs containing $[Tf_2N]$; as previously mentioned, the band related to the $[Tf_2N]$ splits into two bands, which are related to different aggregates, and in the case of $[B(CN)_4]$, the band remains as a single band. However, this finding is consistent with the higher $\Lambda_{exp}/\Lambda_{NMR}$ values obtained for the ILs containing $[B(CN)_4]$, indicating a greater contribution of $Li^+$ to the overall molar ionic conductivity in these ILs. Pure ILs containing $[B(CN)_4]$ and their mixtures with $Li^+$ salt exhibit superior transport properties not only due to the decrease in viscosity but also due to the decrease in aggregate formation between $Li^+$ and the $[B(CN)_4]$ anions given the weak electrostatic interactions between them. This behavior allows the $Li^+$ ions to contribute significantly to the overall ionic conductivity, which is crucial to their use as the electrolyte in lithium ion batteries. The full range of the Raman spectra for $[BMPyr][B(CN)_4]$, $[BMP][B(CN)_4]$, and $[BMMI][B(CN)_4]$ is shown in Figures 15S−17S (SI), respectively.

**Molecular Dynamics Simulations.** MD simulations were performed to evaluate the short-range structure of the neat IL and the $Li^+$ mixture. To compare our results with the literature, $[BMMI][B(CN)_4]$ and its mixture with $Li^+$ were used in this study. The local equilibrium structure was evaluated by the rdf between the center of mass of species $\alpha$ and $\beta$, $g_{\alpha\beta}(r)$.

Figure 9a shows the rdfs of [BMMI]−[BMMI], $[B(CN)_4]$−$[B(CN)_4]$, and the cross term for the neat IL. The rdf profiles

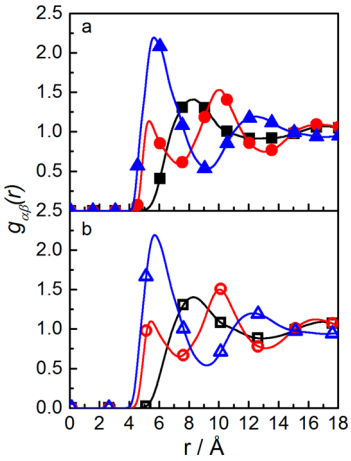


**Figure 9.** The rdf for the center of mass of [BMMI]−[BMMI] (black squares), $[B(CN)_4]$−$[B(CN)_4]$ (red circles), and the cross term (blue triangles) for (a) $[BMMI][B(CN)_4]$ and (b) its $Li^+$ mixture.

suggest a break in the charge ordering present in the ILs because it is possible to observe the first peak of the $[B(CN)_4]$−$[B(CN)_4]$ rdf at a short distance as the cross term rdf at around 5.5 Å. This indicates that the anion has a first coordination shell of other anions closer than the cation. However, the first peak in the $[B(CN)_4]$−$[B(CN)_4]$ rdf has a small intensity, and the number of the neighbor's calculation reveals only 0.30 anions. Therefore, the first coordination shell of $[B(CN)_4]$−$[B(CN)_4]$ is represented by the first two peaks (5.5 and 10 Å) and is composed of 2.0 anions. On the other hand, the [BMMI]−[BMMI] rdf reveals one peak that is related to the first coordination shell at ∼8.2 Å and 1.9 neighboring cations. The cross term rdf is located at ∼5.5 Å, and the number of neighbors is 1.5 ions.

The effect of the addition of $Li^+$ in the IL is shown in Figure 9b. The amount of $Li^+$ added to the IL (0.1 mol $L^{-1}$ or 0.013 molar fraction) is not enough to change the profile of the rdfs as the number of $Li^+$ ions is not statistically significant compared to the IL's ions to have an importance in their surroundings.

To better understand the first peak in the $[B(CN)_4]$−$[B(CN)_4]$ rdf, a combined radial/angular distribution function, cdf, is presented in Figure 10. On the *x*-axis of this cdf is the rdf between the center of the ring of the cation and the B atom of the anion, which is shown at the top of the figure. On the *y*-axis


dx.doi.org/10.1021/jp505051v | J. Phys. Chem. B 2014, 118, 8772−8781

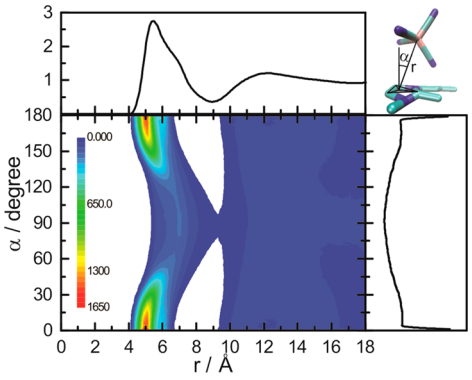


**Figure 10.** Combined radial/angular distribution function of the center of the cation ring and the anion center of mass. The angle is between a vector perpendicular to the cation ring plane and a vector from the anion center of mass to the center of the cation ring.

is the adf of the angle formed between a vector from the center of the ring to the B atom and a vector that is perpendicular to the ring plane (see the cartoon on the right side of Figure 10). The colors represent the occurrence of both distributions. It is possible to see that the anions are in general at 0 and 180° with respect to the ring plane, as indicated by the first peak (~5.0 Å). This means that the majority of anions have between them one cation, resulting in a bigger distance between them, as revealed by the second peak in the $[B(CN)_4]-[B(CN)_4]$ rdf. However, note that there is some probability to find anions at 90° to the ring plane. These anions are closer to the anions at 0 and 180° and give rise to the first peak in the $[B(CN)_4]-[B(CN)_4]$ rdf. The peak intensity is lower in this case; therefore, the probability to find an anion at this position is also lower, and only some configurations will be found in this arrangement. Consequently, the first peak in the $[B(CN)_4]-[B(CN)_4]$ rdf has a low intensity and is due to only 0.3 anions.

This feature is clearly observed in Figure 11, which shows the sdf of the counterion center of mass around the other ion in the neat IL in two different probability levels. Figure 11a and c shows the anion center of mass around the cation with higher probability density and lower probability density, respectively. As already indicated by the cdf, the anions lie above and under the cation ring with higher density, but it is also possible to find anions in other positions with a lower probability density. Figure 11b and d shows the cation center of mass around the anion with higher probability density and lower probability density, respectively. The cations are spread out around the anion between two atoms of N because the $[B(CN)_4]$ anion is highly symmetrical.

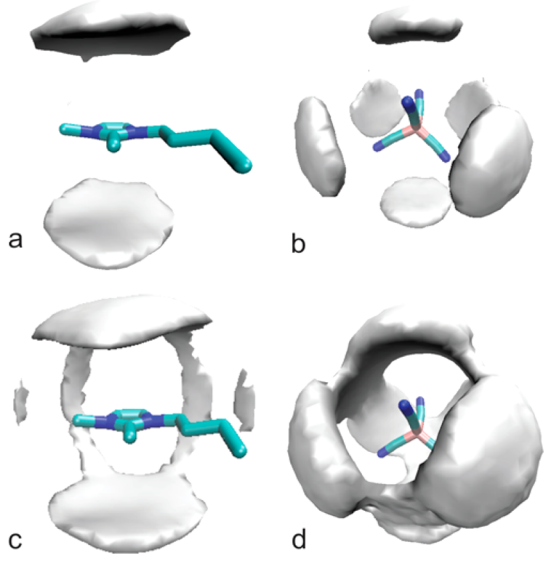


**Figure 11.** The sdf of the center of mass of (a,c) the anion around the cation and (b,d) the cation around the anion, with (a,b) higher probability density and (c,d) lower probability density.

Figure 12a shows the local structure of the metallic cation in the $Li^+$ mixture, and the rdfs of the center of mass of $Li^+-Li^+$,

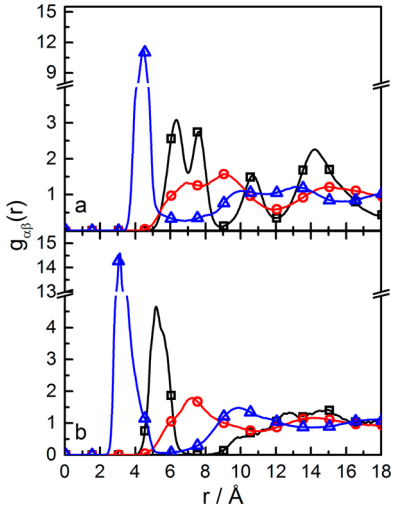


**Figure 12.** The rdf for the center of mass of $Li^+-Li^+$ (black squares), $Li^+-[BMMI]$ (red circles), and $Li^+-$anion (blue triangles) for (a) $[Li][BMMI][B(CN)_4]$ and (b) $[Li][BMMI][Tf_2N]$.

$Li^+-[BMMI]$, and $Li^+-[B(CN)_4]$ are presented. As expected, despite the low coordinating ability of $[B(CN)_4]$, the closest ion from $Li^+$ is the anion. The first coordination peak is located at 4.5 Å, and it corresponds to 4.3 anions. The literature contains studies with $[Tf_2N]$ but with higher $Li^+$ concentration.[8,10,13,52] For a better comparison, a similar system, but using the $[Tf_2N]$ anion, was simulated with the same conditions and number of ions. Figure 12b shows rdfs of the center of mass of $Li^+-Li^+$, $Li^+-[BMMI]$, and $Li^+-[Tf_2N]$. The ion closest to $Li^+$ is also the anion, and the first peak is located at 3.0 Å and corresponds to 3.1 anions. The fact that the $[B(CN)_4]$ anion has lower coordinating ability than $[Tf_2N]$ results in a coordination sphere with more $[B(CN)_4]$ than $[Tf_2N]$ because more $[B(CN)_4]$ is necessary to equilibrate the charges. In addition, one must take into consideration the fact that the $[Tf_2N]$ anion presents four O atoms in its structure and it can bicoordinate with the $Li^+$.[10] Moreover, the $[B(CN)_4]$ anions are 45% more distant than the $[Tf_2N]$ anions. The weaker interaction between the $[B(CN)_4]$ anion and the $Li^+$ guarantees a higher distance between the ions. One can have a better picture of the $Li^+$ coordination by observing Figure 18S (SI). It shows the rdf between the metallic cation and the closest atom of the anion; in the case of $[B(CN)_4]$, the peak related to the closest N is located at 2.0 Å, and in the case of the $[Tf_2N]$, the peak related to the closest O is located at 1.8 Å. These results are in line with the physicochemical properties that suggest a weaker interaction between $Li^+$ and $[B(CN)_4]$


dx.doi.org/10.1021/jp505051v | J. Phys. Chem. B 2014, 118, 8772−8781

than that between $Li^+$ and $[Tf_2N]$ and explain the higher mobility of $Li^+$ in ILs containing the $[B(CN)_4]$ anion.

## CONCLUSIONS

In conclusion, these results show that the transport properties of ILs can be manipulated by changing the coordinating properties of the anions used. This provides much room for future research in which the ionic transport due to $Li^+$ can be drastically improved. The ILs tailored in this work show superior transport properties not only related to the diminution of viscosity but also because of the decrease in the formation of aggregates between $Li^+$ and the $[B(CN)_4]$ anion due to the weak electrostatic and short-range interactions between them. MD simulations support the weaker interaction between $Li^+$ and the $[B(CN)_4]$ anion than that with the $[Tf_2N]$ anion. This behavior leads to an important contribution of $Li^+$ to the ionic conductivity that could expand the range of applications where they can be utilized, assuring their position as an important technology advancement in the future of energy storage.

## ASSOCIATED CONTENT

### Supporting Information

$^{13}C$ NMR of $KB(CN)_4$ is presented in Figure 1S. $^1H$ and $^{13}C$ NMRs of $[BMPyr][B(CN)_4]$, $[BMP][B(CN)_4]$, and $[BMMI][B(CN)_4]$ are presented in Figure 2S−7S, respectively. Table 1S presents the systems simulated by MD. Figure 8S presents the typical energy fluctuation in the MD simulations. TG and DSC analyses are show in Figures 9S and 10S, respectively. EWs are showed in Figure 11S. Table 2S presents the VTF parameters for viscosity. Figure 12S presents the Walden plot for the ILs containing $[B(CN)_4]$. Figure 13S presents the plot of self-diffusion coefficients as a function of the fluidity. Figure 14S presents the molar ionic conductivity calculated experimentally and by the self-diffusion coefficient. Figures 15S−17S present the infrared and Raman spectra of $[BMPyr][B(CN)_4]$, $[BMP][B(CN)_4]$, and $[BMMI][B(CN)_4]$, respectively. Figure 18S presents the rdf between $Li^+$ and the closest atom of the anions. All physicochemical data are present in Table 3S and 4S. This material is available free of charge via the Internet at http://pubs.acs.org.

## AUTHOR INFORMATION

### Corresponding Author

*E-mail: rtorresi@iq.usp.br. Phone: +55-11-30919194. Fax: +55-11-38155640.

### Author Contributions

⊥N.S.-R. and V.L.M. have contributed equally to this paper. The manuscript was written through contributions of all authors. All authors have given approval to the final version of the manuscript.

### Notes

The authors declare no competing financial interest.

## ACKNOWLEDGMENTS

The authors acknowledge FAPESP (09/53199-3) for financial support. N.S.-R. and V.L.M. thank FAPESP (10/08646-9 and 13/22748-7, respectively) for fellowship support.

## REFERENCES

(1) MacFarlane, D. R.; Forsyth, M.; Howlett, P. C.; Pringle, J. M.; Sun, J.; Annat, G.; Neil, W.; Izgorodina, E. I. Ionic Liquids in Electrochemical Devices and Processes: Managing Interfacial Electrochemistry. *Acc. Chem. Res.* **2007**, *40*, 1165−73.

(2) Armand, M.; Endres, F.; MacFarlane, D. R.; Ohno, H.; Scrosati, B. Ionic-Liquid Materials for the Electrochemical Challenges of the Future. *Nat. Mater.* **2009**, *8*, 621−629.

(3) Fraser, K. J.; MacFarlane, D. R. Phosphonium-Based Ionic Liquids: An Overview. *Aust. J. Chem.* **2009**, *62*, 309.

(4) Rennie, A. J. R.; Sanchez-Ramirez, N.; Torresi, R. M.; Hall, P. J. Ether-Bond-Containing Ionic Liquids as Supercapacitor Electrolytes. *J. Phys. Chem. Lett.* **2013**, *4*, 2970−2974.

(5) Benedetti, T. M.; Gonçales, V. R.; Córdoba de Torresi, S. I.; Torresi, R. M. In Search of an Appropriate Ionic Liquid as Electrolyte for Macroporous Manganese Oxide Film Electrochemistry. *J. Power Sources* **2013**, *239*, 1−8.

(6) Wang, Y.; Zaghib, K.; Guerfi, A.; Bazito, F. F. C.; Torresi, R. M.; Dahn, J. R. Accelerating Rate Calorimetry Studies of the Reactions between Ionic Liquids and Charged Lithium Ion Battery Electrode Materials. *Electrochim. Acta* **2007**, *52*, 6346−6352.

(7) Kim, G.-T.; Jeong, S. S.; Xue, M.-Z.; Balducci, A.; Winter, M.; Passerini, S.; Alessandrini, F.; Appetecchi, G. B. Development of Ionic Liquid-Based Lithium Battery Prototypes. *J. Power Sources* **2012**, *199*, 239−246.

(8) Fujii, K.; Hamano, H.; Doi, H.; Song, X.; Tsuzuki, S.; Hayamizu, K.; Seki, S.; Kameda, Y.; Dokko, K.; Watanabe, M.; Umebayashi, Y. Unusual Li + Ion Solvation Structure in Bis(fluorosulfonyl)amide Based Ionic Liquid. *J. Phys. Chem. C* **2013**, *117*, 19314−19324.

(9) MacFarlane, D. R.; Tachikawa, N.; Forsyth, M.; Pringle, J. M.; Howlett, P. C.; Elliott, G. D.; Davis, J. H.; Watanabe, M.; Simon, P.; Angell, C. A. Energy Applications of Ionic Liquids. *Energy Environ. Sci.* **2014**, *7*, 232−250.

(10) Monteiro, M. J.; Bazito, F. F. C.; Siqueira, L. J. A.; Ribeiro, M. C. C.; Torresi, R. M. Transport Coefficients, Raman Spectroscopy, and Computer Simulation of Lithium Salt Solutions in an Ionic Liquid. *J. Phys. Chem. B* **2008**, *112*, 2102−2109.

(11) Monteiro, M. J.; Camilo, F. F.; Ribeiro, M. C. C.; Torresi, R. M. Ether-Bond-Containing Ionic Liquids and the Relevance of the Ether Bond Position to Transport Properties. *J. Phys. Chem. B* **2010**, *114*, 12488−12494.

(12) Ueno, K.; Tokuda, H.; Watanabe, M. Ionicity in Ionic Liquids: Correlation with Ionic Structure and Physicochemical Properties. *Phys. Chem. Chem. Phys.* **2010**, *12*, 1649−1658.

(13) Umebayashi, Y.; Harnano, H.; Seki, S.; Minofar, B.; Fujii, K.; Hayamizu, K.; Tsuzuki, S.; Kameda, Y.; Kohara, S.; Watanabe, M. Liquid Structure of and $Li^+$ Ion Solvation in Bis-(trifluoromethanesulfonyl)amide Based Ionic Liquids Composed of 1-Ethyl-3-methylimidazolium and *N*-Methyl-*N*-propylpyrrolidinium Cations. *J. Phys. Chem. B* **2011**, *115*, 12179−12191.

(14) Scheers, J.; Pitawala, J.; Thebault, F.; Kim, J.-K.; Ahn, J.-H.; Matic, A.; Johansson, P.; Jacobsson, P. Ionic Liquids and Oligomer Electrolytes Based on the $B(CN)_4^-$ Anion; Ion Association, Physical and Electrochemical Properties. *Phys. Chem. Chem. Phys.* **2011**, *13*, 14953−14959.

(15) Marszalek, M.; Fei, Z.; Zhu, D.-R.; Scopelliti, R.; Dyson, P. J.; Zakeeruddin, S. M.; Grätzel, M. Application of Ionic Liquids Containing Tricyanomethanide $[C(CN)_3]^-$ or Tetracyanoborate $[B(CN)_4]^-$ Anions in Dye-Sensitized Solar Cells. *Inorg. Chem.* **2011**, *50*, 11561−11567.

(16) Kuang, D.; Wang, P.; Ito, S.; Zakeeruddin, S. M.; Grätzel, M. Stable Mesoscopic Dye-Sensitized Solar Cells Based on Tetracyanoborate Ionic Liquid Electrolyte. *J. Am. Chem. Soc.* **2006**, *128*, 7732−7733.

(17) Scheers, J.; Johansson, P.; Jacobsson, P. Anions for Lithium Battery Electrolytes: A Spectroscopic and Theoretical Study of the $B(CN)_4^-$ Anion of the Ionic Liquid $C_2^{mim}[B(CN)_4]$. *J. Electrochem. Soc.* **2008**, *155*, A628−A634.

(18) Koller, T. M.; Rausch, M. H.; Ramos, J.; Schulz, P. S.; Wasserscheid, P.; Economou, I. G.; Fröba, A. P. Thermophysical Properties of the Ionic Liquids $[EMIM][B(CN)_4]$ and $[HMIM][B(CN)_4]$. *J. Phys. Chem. B* **2013**, *117*, 8512−8523.

(19) Pandey, G. P.; Hashmi, S. A. Studies on Electrical Double Layer Capacitor with a Low-Viscosity Ionic Liquid 1-Ethyl-3-methylimidazolium Tetracyanoborate as Electrolyte. *Bull. Mater. Sci.* **2013**, *36*, 729−733.
(20) Koller, T.; Rausch, M. H.; Schulz, P. S.; Berger, M.; Wasserscheid, P.; Economou, I. G.; Leipertz, A.; Fröba, A. P. Viscosity, Interfacial Tension, Self-Diffusion Coefficient, Density, and Refractive Index of the Ionic Liquid 1-Ethyl-3-methylimidazolium Tetracyanoborate as a Function of Temperature at Atmospheric Pressure. *J. Chem. Eng. Data* **2012**, *57*, 828−835.
(21) Bazito, F. F. C.; Kawano, Y.; Torresi, R. M. Synthesis and Characterization of Two Ionic Liquids with Emphasis on Their Chemical Stability Towards Metallic Lithium. *Electrochim. Acta* **2007**, *52*, 6427−6437.
(22) Bernhardt, E.; Finze, M.; Willner, H. Eine Effiziente Synthese von Tetracyanoboraten Durch Sinterprozesse. *Z. Anorg. Allg. Chem.* **2003**, *629*, 1229−1234.
(23) Küppers, T.; Bernhardt, E.; Willner, H.; Rohm, H. W.; Köckerling, M. Tetracyanoborate Salts $M[B(CN)_4]$ with M = Singly Charged Cations: Properties and Structures. *Inorg. Chem.* **2005**, *44*, 1015−1022.
(24) Monteiro, M. J.; Ando, R. A.; Siqueira, L. J. A.; Camilo, F. F.; Santos, P. S.; Ribeiro, M. C. C.; Torresi, R. M. Effect of $SO_2$ on the Transport Properties of an Imidazolium Ionic Liquid and Its Lithium Solution. *J. Phys. Chem. B* **2011**, *115*, 9662−70.
(25) Morrow, T. I.; Maginn, E. J. Molecular Dynamics Study of the Ionic Liquid 1-*N*-Butyl-3-methylimidazolium Hexafluorophosphate. *J. Phys. Chem. B* **2002**, *106*, 12807−12813.
(26) Koller, T.; Ramos, J.; Garrido, N. M.; Fröba, A. P.; Economou, I. G. Development of a United-Atom Force Field for 1-Ethyl-3-methylimidazolium Tetracyanoborate Ionic Liquid. *Mol. Phys.* **2012**, *110*, 1115−1126.
(27) Martínez, L.; Andrade, R.; Birgin, E. G.; Martínez, J. M. PACKMOL: A Package for Building Initial Configurations for Molecular Dynamics Simulations. *J. Comput. Chem.* **2009**, *30*, 2157−2164.
(28) Swope, W. C.; Andersen, H. C.; Berens, P. H.; Wilson, K. R. A Computer Simulation Method for the Calculation of Equilibrium Constants for the Formation of Physical Clusters of Molecules: Application to Small Water Clusters. *J. Chem. Phys.* **1982**, *76*, 637−649.
(29) Figueirido, F.; Levy, R. M.; Zhou, R.; Berne, B. J. Large Scale Simulation of Macromolecules in Solution: Combining the Periodic Fast Multipole Method with Multiple Time Step Integrators. *J. Chem. Phys.* **1997**, *106*, 9835−9849.
(30) Urahata, S. M.; Ribeiro, M. C. C. Structure of Ionic Liquids of 1-Alkyl-3-methylimidazolium Cations: A Systematic Computer Simulation Study. *J. Chem. Phys.* **2004**, *120*, 1855−1863.
(31) Brehm, M.; Kirchner, B. TRAVIS - A Free Analyzer and Visualizer for Monte Carlo and Molecular Dynamics Trajectories. *J. Chem. Inf. Model.* **2011**, *51*, 2007−2023.
(32) Vranes, M.; Dozic, S.; Djeric, V.; Gadzuric, S. Physicochemical Characterization of 1-Butyl-3-methylimidazolium and 1-Butyl-1-methylpyrrolidinium Bis(trifluoromethylsulfonyl)imide. *J. Chem. Eng. Data* **2012**, *57*, 1072−1077.
(33) Ngo, H. L.; LeCompte, K.; Hargens, L.; McEwen, A. B. Thermal Properties of Imidazolium Ionic Liquids. *Thermochim. Acta* **2000**, *357*−*358*, 97−102.
(34) Endres, F.; Zein El Abedin, S. Air and Water Stable Ionic Liquids in Physical Chemistry. *Phys. Chem. Chem. Phys.* **2006**, *8*, 2101−2116.
(35) Geppert-Rybczyńska, M.; Lehmann, J. K.; Heintz, A. Physicochemical Properties of Two 1-Alkyl-1-methylpyrrolidinium Bis[(trifluoromethyl)sulfonyl]imide Ionic Liquids and of Binary Mixtures of 1-Butyl-1-methylpyrrolidinium Bis[(trifluoromethyl)-sulfonyl]imide with Methanol or Acetonitrile. *J. Chem. Thermodyn.* **2014**, *71*, 171−181.
(36) Martins, V. L.; Sanchez-Ramírez, N.; Calderon, J. A.; Torresi, R. M. Electrochemistry of Copper in Ionic Liquids with Different Coordinating Properties. *J. Mater. Chem. A* **2013**, *1*, 14177−14182.
(37) Ye, C.; Shreeve, J. M. Rapid and Accurate Estimation of Densities of Room-Temperature Ionic Liquids and Salts. *J. Phys. Chem. A* **2007**, *111*, 1456−1461.
(38) Harris, K. R.; Woolf, L. A.; Kanakubo, M.; Rüther, T. Transport Properties of *N*-Butyl-*N*-methylpyrrolidinium Bis-(trifluoromethylsulfonyl)amide. *J. Chem. Eng. Data* **2011**, *56*, 4672−4685.
(39) Angell, C. A. Liquid Fragility and the Glass Transition in Water and Aqueous Solutions. *Chem. Rev.* **2002**, *102*, 2627−2650.
(40) Ribeiro, M. C. C. Low-Frequency Raman Spectra and Fragility of Imidazolium Ionic Liquids. *J. Chem. Phys.* **2010**, *133*, 024503.
(41) MacFarlane, D. R.; Forsyth, M.; Izgorodina, E. I.; Abbott, A. P.; Annat, G.; Fraser, K. On the Concept of Ionicity in Ionic Liquids. *Phys. Chem. Chem. Phys.* **2009**, *11*, 4962−4967.
(42) Austen Angell, C.; Ansari, Y.; Zhao, Z. Ionic Liquids: Past, Present and Future. *Faraday Discuss.* **2012**, *154*, 9−27.
(43) Xu, W.; Cooper, E. I.; Angell, C. A. Ionic Liquids: Ion Mobilities, Glass Temperatures, and Fragilities. *J. Phys. Chem. B* **2003**, *107*, 6170−6178.
(44) Gardas, R. L.; Costa, H. F.; Freire, M. G.; Carvalho, P. J.; Marrucho, I. M.; Fonseca, I. M. A.; Ferreira, A. G. M.; Coutinho, J. A. P. Densities and Derived Thermodynamic Properties of Imidazolium-, Pyridinium-, Pyrrolidinium-, and Piperidinium-Based Ionic Liquids. *J. Chem. Eng. Data* **2008**, *53*, 805−811.
(45) Herriot, C.; Khatun, S.; Fox, E. T.; Judeinstein, P.; Armand, M.; Henderson, W. A.; Greenbaum, S. Diffusion Coefficients from $^{13}C$ PGSE NMR Measurements—Fluorine-Free Ionic Liquids with the DCTA−Anion. *J. Phys. Chem. Lett.* **2012**, *3*, 441−444.
(46) Blanchard, J. W.; Beliéres, J.-P.; Alam, T. M.; Yarger, J. L.; Holland, G. P. NMR Determination of the Diffusion Mechanisms in Triethylamine-Based Protic Ionic Liquids. *J. Phys. Chem. Lett.* **2011**, *2*, 1077−1081.
(47) Castiglione, F.; Ragg, E.; Mele, A.; Appetecchi, G. B.; Montanino, M.; Passerini, S. Molecular Environment and Enhanced Diffusivity of $Li^+$ Ions in Lithium-Salt-Doped Ionic Liquid Electrolytes. *J. Phys. Chem. Lett.* **2011**, *2*, 153−157.
(48) Lassegues, J.-C.; Grondin, J.; Talaga, D. Lithium Solvation in Bis(trifluoromethanesulfonyl)imide-Based Ionic Liquids. *Phys. Chem. Chem. Phys.* **2006**, *8*, 5629−5632.
(49) Duluard, S.; Grondin, J.; Bruneel, J.-L.; Pianet, I.; Grélard, A.; Campet, G.; Delville, M.-H.; Lassègues, J.-C. Lithium Solvation and Diffusion in the 1-Butyl-3-methylimidazolium Bis-(trifluoromethanesulfonyl)imide Ionic Liquid. *J. Raman Spectrosc.* **2008**, *39*, 627−632.
(50) Castriota, M.; Caruso, T.; Agostino, R. G.; Cazzanelli, E.; Henderson, W. A.; Passerini, S. Raman Investigation of the Ionic Liquid *N*-Methyl-*N*-propylpyrrolidinium Bis-(trifluoromethanesulfonyl)imide and Its Mixture with $LiN(SO_2CF_3)_2$. *J. Phys. Chem. A* **2005**, *109*, 92−96.
(51) Mao, J. X.; Lee, A. S.; Kitchin, J. R.; Nulwala, H. B.; Luebke, D. R.; Damodaran, K. Interactions in 1-Ethyl-3-methyl Imidazolium Tetracyanoborate Ion Pair: Spectroscopic and Density Functional Study. *J. Mol. Struct.* **2013**, *1038*, 12−18.
(52) Umebayashi, Y.; Mori, S.; Fujii, K.; Tsuzuki, S.; Seki, S.; Hayamizu, K.; Ishiguro, S. Raman Spectroscopic Studies and Ab Initio Calculations on Conformational Isomerism of 1-Butyl-3-methylimidazolium Bis-(trifluoromethanesulfonyl)amide Solvated to a Lithium Ion in Ionic Liquids: Effects of the Second Solvation Sphere of the Lithium Ion. *J. Phys. Chem. B* **2010**, *114*, 6513−6521.